Phase diagram of a long bar under a higher-order active contour energy: application to hydrographic network extraction from VHR satellite images.

Aymen El Ghoul, Ian Jermyn, Josiane Zerubia

▶ **To cite this version:**

Aymen El Ghoul, Ian Jermyn, Josiane Zerubia. Phase diagram of a long bar under a higher-order active contour energy: application to hydrographic network extraction from VHR satellite images.. ICPR, Dec 2008, Tampa, Floride, United States. inria-00316619

HAL Id: inria-00316619
https://inria.hal.science/inria-00316619

Submitted on 3 Sep 2008

HAL is a multi-disciplinary open access archive for the deposit and dissemination of scientific research documents, whether they are published or not. The documents may come from teaching and research institutions in France or abroad, or from public or private research centers.

L'archive ouverte pluridisciplinaire **HAL**, est destinée au dépôt et à la diffusion de documents scientifiques de niveau recherche, publiés ou non, émanant des établissements d'enseignement et de recherche français ou étrangers, des laboratoires publics ou privés.

Phase diagram of a long bar under a higher-order active contour energy: application to hydrographic network extraction from VHR satellite images

Aymen El Ghoul, Ian H. Jermyn and Josiane Zerubia
ARIANA - Joint Team-Project INRIA/CNRS/UNSA
2004 route des Lucioles, BP 93, 06902 Sophia Antipolis Cedex, France
{*Aymen.El_Ghoul, Ian.Jermyn, Josiane.Zerubia*}*@sophia.inria.fr*

Abstract

The segmentation of networks is important in several imaging domains, and models incorporating prior shape knowledge are often essential for the automatic performance of this task. Higher-order active contours provide a way to include such knowledge, but their behaviour can vary significantly with parameter values: e.g. *the same energy can model networks or a 'gas of circles'. In this paper, we present a stability analysis of a HOAC energy leading to the phase diagram of a long bar. The results, which are confirmed by numerical experiments, enable the selection of parameter values for the modelling of network shapes using the energy. We apply the resulting model to the problem of hydrographic network extraction from VHR satellite images.*

1. Introduction

Water is a critical resource, and likely to become more so in the future. Consequently, the ability to monitor water resources is of great importance. One way to perform such monitoring is through the use of remote sensing imagery, and in particular, very high resolution (VHR) satellite images. Many organizations that deal with such images are therefore interested in automatic processing that allows water resources to be measured and evaluated. In this paper, we focus on the segmentation of hydrographic networks from VHR satellite images. This is a difficult problem, because such networks are frequently not distinguishable from the background by local image measurements alone. Rather, it is the 'shape' of the region in the image domain occupied by the network that distinguishes them: networks occupy regions in the image domain composed of a set of 'arms' that join together at junctions. There has been a significant amount of work on shape modelling for segmentation, but most of this work models shape by comparing the region sought to a reference regions or regions [1, 7]. This works well for many applications, but is not appropriate when the region sought can have an arbitrary topology, as is the case for networks. To model such regions, 'higher-order active contours' (HOACs) were introduced [5]. Unlike the original active contours [4] and their successors, this new generation of active contours incorporates non-trivial shape information about the region being modelled via long-range interactions between region boundary points.

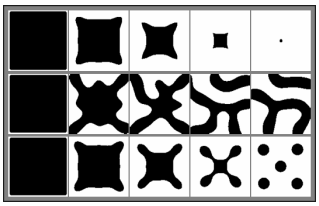

Figure 1. Gradient descent evolutions (from left to right) for different parameter values in the HOAC model of [5].

The HOAC prior energy defined in [5] was used to model network-shaped regions. However, it was soon discovered that it could be used to model other families of regions too, notably a 'gas of circles' (regions composed of an arbitrary number of approximate circles [3]), simply by varying the model parameters. Figure 1 illustrates these different behaviours. Thus, in order to use the model for network segmentation, for example, it is important to know which parameter ranges lead to stable network regions, as opposed, for example, to stable 'gas of circles' regions.

This paper addresses this issue by performing a stability analysis of the prior HOAC energy introduced

in [5].[1] Ideally, the stability of an arbitrary network shape should be analysed, but this is an extremely complex problem. However, network shapes are essentially composed of basic components: 'arms', which are relatively long and have low curvature on the scale of their width, and 'junctions'. The most important type of stability concerns the arms, since without arms there can be no network. A tractable and reasonable approximation therefore seems to be to analyse the stability of a long, straight bar, which is the subject of this paper.

We first Taylor-expand the HOAC energy around a long bar configuration to second order. We then impose stability conditions: the first functional derivative should be zero (a long bar is an energy extremum) and the second functional derivative should be positive definite (the extremum is a minimum). These conditions constrain the values of the parameters. The results can be summarized in a 'phase diagram' illustrating the zone in parameter space leading to stable bars.

Such stability analyses will become more important as region models become more sophisticated, which is inevitable if automatic solutions to segmentation problems are to be found. The interest of the calculation is thus not limited to the current model, or even to HOAC models in general.

In Section 2, we perform the Taylor expansion and stability analysis. In Section 3, we confirm the results of the stability analysis via numerical experiments; then, adding a likelihood energy, we describe an experiment on a satellite image. We conclude in Section 4.

2 Theory

The prior HOAC energy introduced in [5] is

$$E_G(R) = \lambda_C L(R) + \alpha_C A(R) - \frac{\beta_C}{2} \iint dt\, dt'\, \dot\gamma(t) \cdot \dot\gamma(t')\, \Phi(\sigma(t,t')/d)\ , \qquad (1)$$

where R is a region in the image domain; L is region boundary length; A is region area; γ is an embedding representing the region boundary, parameterized by t; $\dot\gamma$ is its derivative, *i.e.* the tangent vector field; Φ defines the interaction between two boundary points separated by a distance $\sigma(t,t') = |\gamma(t) - \gamma(t')|$; and λ_C, α_C, β_C, and d are real parameters. In particular, d controls the interaction range. The long-range interaction is responsible for the prior shape information.

Our aim is to find the ranges of α_C and β_C (without loss of generality we can put $\lambda_C = d = 1$) for which a long bar is stable, *i.e.* is a local minimum of this energy. To begin, we Taylor expand the energy around a long bar.

[1] A preliminary version of this work was published in French [2].

2.1 Taylor expansion around a long bar

The second-order Taylor expansion of E_G is

$$E_G^{(2)}(\gamma) = E_G^{(2)}(\gamma_0 + \delta\gamma) \triangleq E_G(\gamma_0) + \langle \delta\gamma | \frac{\delta E_G}{\delta\gamma}\Big|_{\gamma_0} \rangle + \frac{1}{2} \langle \delta\gamma | \frac{\delta^2 E_G}{\delta\gamma^2}\Big|_{\gamma_0} | \delta\gamma \rangle\ , \qquad (2)$$

where $\langle \cdot | \cdot \rangle$ is a metric defined over the space of embeddings, and $\delta\gamma$ is a small perturbation of γ_0. The configuration γ_0 is stable if and only if $\frac{\delta E_G}{\delta\gamma}|_{\gamma_0} = 0$, *i.e.* if γ_0 is an extremum of E_G, and the Hessian matrix $\frac{\delta^2 E_G}{\delta\gamma^2}|_{\gamma_0}$ is positive definite, *i.e.* the extremum is a minimum.

A bar, γ_0, of length l and width w_0, is given by

$$\gamma_{0,\mu}(t_\mu) = \begin{cases} x_{0,\mu}(t_\mu) = \pm_\mu l t_\mu & t_\mu \in [-\frac{1}{2}, \frac{1}{2}] \\ y_{0,\mu}(t_\mu) = \pm_\mu \frac{w_0}{2} & . \end{cases} \qquad (3)$$

The bar can be viewed as periodic in x with period l, and has two boundary components, indicated by $\mu = 1$ or 2. The symbol $\pm_\mu = 1$ if $\mu = 1$ and -1 if $\mu = 2$.

Perturbations of the bar $\delta\gamma$ are defined by tangential and normal changes in the boundary components: $\delta\gamma_\mu(t_\mu) = (\delta x_\mu(t_\mu), \delta y_\mu(t_\mu))$. Tangential changes do not change the bar's shape and hence do not change the energy; we can therefore set $\delta x_\mu = 0$. The Hessian matrix is diagonal in the Fourier basis of the tangent space at γ_0 [2], so it is useful to express $\delta\gamma$ in this basis: $\delta y_\mu(t_\mu) = \sum_{k_\mu} a_{\mu,k_\mu} e^{i k_\mu l t_\mu}$, where $k_\mu = \frac{2\pi m_\mu}{l}$ for $m_\mu \in \mathbb{Z}$.

After some calculation, we find [2]

$$\begin{aligned} e_G^{(2)}(\gamma) \triangleq \frac{E_G^{(2)}(\gamma)}{l} &\simeq \underbrace{2 + \alpha_C w_0 - \beta_C G_{00}(w_0)}_{e_0} \\ &+ [a_{1,0} - a_{2,0}] \underbrace{[\alpha_C - \beta_C G_{10}(w_0)]}_{e_1} \\ &+ \frac{1}{2} \sum_k \left[|a_{1,k}|^2 + |a_{2,k}|^2 \right] \underbrace{\left[k^2 + \beta_C G_{20}(w_0, k) \right]}_{e_{20}} \\ &+ (a_{1,k} a_{2,k} + a_{1,-k} a_{2,-k}) \underbrace{\beta_C G_{21}(w_0, k)}_{e_{21}} \\ &= e_0 + e_1 (a_{1,0} - a_{2,0}) + \frac{1}{2} \sum_k a_k^\dagger\, e_2\, a_k\ , \end{aligned} \qquad (4)$$

where $a_k = (a_{1,k}^*, a_{2,k})$; $\dagger$ and $*$ indicate respectively Hermitian and complex conjugates; and the $G(w_0, k)$ depend on Φ. $e_0(w_0)$ is the energy per unit length of a long bar of width w_0, while $e_1(w_0) = \partial e_0(w_0)/\partial w_0$ is the change in energy due to a change in width (to first order, non-zero Fourier frequencies do not contribute). $e_2(w_0, k)$ is, for each frequency k, a symmetric 2×2

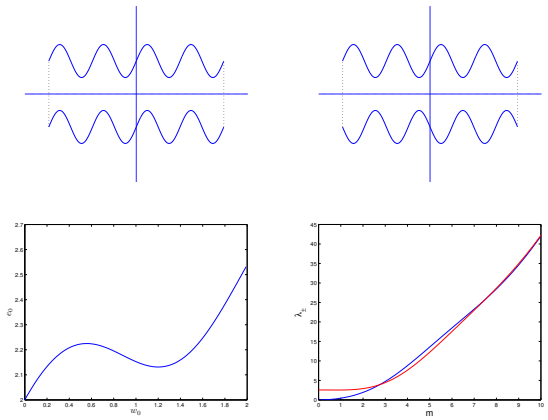

Figure 2. Top: left, example of a^+; right, example of a^-. Bottom: left, bar energy against w_0, with minimum at $w_0^* = 1.2$; right, λ_+ (blue) and λ_- (red) against frequency. Parameters: $\alpha_C = 0.8$, $\beta_C = 0.53$. Note $\lambda_\pm > 0\ \forall k$.

matrix whose diagonal and off-diagonal terms, e_{20} and e_{21}, express the self-energy of perturbations of one side, and the interaction between perturbations of opposite sides of the bar respectively.

2.2 Stability analysis of a long bar

The condition that $\delta E_G/\delta\gamma = 0$, *i.e.* that $e_1 = 0$, determines β_C in terms of α_C and w_0:

$$\beta_C(\alpha_C, w_0) = \frac{\alpha_C}{G_{10}(w_0)}\ . \tag{5}$$

The condition that the Hessian be positive definite, *i.e.* that the eigenvalues of e_2 be strictly positive for all frequencies, allows us to find lower and upper bounds on α_C [2]. The eigenvectors of e_2 are $v_\pm = (1, \pm 1)$, with eigenvalues $\lambda_{\pm,k} = e_{20}(k) \pm e_{21}(k)$ respectively. Equation (4) can be written in terms of $\lambda_\pm$:

$$e_G^{(2)} = e_0 + e_1(a_{1,0} - a_{2,0}) + \frac{1}{4}\sum_k \lambda_{+,k}|a_k^+|^2 + \lambda_{-,k}|a_k^-|^2$$

where $a_k^\pm = a_{1,k} \pm a_{2,k}^*$. These eigenmodes are illustrated in Figure 2: a^+ describes in-phase perturbations of the two sides, while a^- describes out-of-phase perturbations. For low frequencies, the former cost less energy, as locally the sides of the shape are still parallel. For higher frequencies, the difference is negligible.

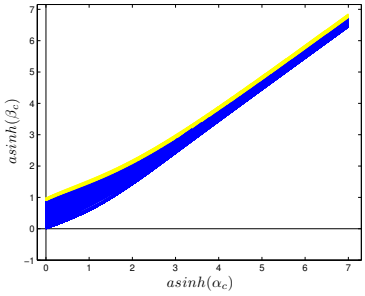

Figure 3. Phase diagram: zone in the (α, β) plane allowing a stable bar. Blue: $e_G^{(2)} > 0$; yellow: $e_G^{(2)} < 0$.

A minimum in the energy exists only for $w_0 \in (0.88, 2)$ due to the form of Φ [2]. Using equation (5), we can plot β_C against α_C for $w_0 \in (0.88, 2)$, between the upper and lower bounds on α_C. The result is a 2D zone in the (α, β) plane, illustrated in Figure 3, in which the parameter values permit a stable bar. Since the total energy is $E_G^{(2)}(\gamma) = l e_G^{(2)}(\gamma)$, the behaviour of a long bar depends on the sign of $e_G^{(2)}(\gamma)$. If $e_G^{(2)} > 0$, the bar will shorten and either form a stable circle or disappear. If $e_G^{(2)} < 0$, the bar will elongate, without limit if the domain is unbounded. The blue and yellow zones in Figure 3 correspond to $e_G^{(2)} > 0$ and $e_G^{(2)} < 0$ respectively. Below the coloured zone, the dominant instability is change in w_0: in gradient descent, the bar should get thinner and disappear. Above the coloured zone, the dominant instability is at non-zero frequencies: the bar should develop oscillations and break up. These results will be confirmed numerically in Section 3.1.

3 Experiment

We first present gradient descent evolution experiments using E_G (not $E_G^{(2)}$) to confirm the results of the analysis in Section 2. We then add a likelihood term, and test the energy on a real image.

3.1 Geometric evolution

Figure 4 shows five gradient descent evolutions starting from a long bar. The parameter values for the rows of Figure 4 were $(w_0, \alpha_C, \beta_C, d)$ = $(0, 0.052, 0.02, 10)$, $(10, 0.067, 0.053, 7.75)$, $(30, 8.48, 6.28, 23.8)$, $(20, 8.02, 6.56, 15.26)$, and $(25, 0.319, 2.4, 11.36)$. The following points correspond to these rows: 1) parameters chosen from below

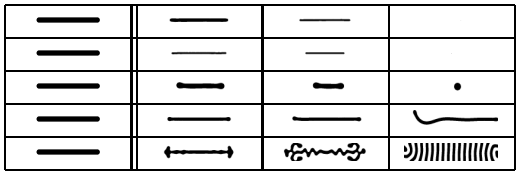

Figure 4. Gradient descent evolutions starting from a bar for parameter values from different zones in figure 3.

the coloured zone; the bar is unstable to changes in its width, and so it thins and disappears; 2) parameters chosen from the blue zone; the bar is stable, but has positive energy per unit length, so it shortens and disappears; 3) parameters again chosen from the blue zone; the bar shortens, but rather than disappear, it evolves to a stable circle [3]; 4) parameters chosen from the yellow zone; the bar has negative energy per unit length, so it elongates, and then buckles due to the finite size of the domain; 5) parameters chosen from above the coloured zone; the bar is unstable to non-zero frequencies, so it develops oscillations and then breaks up; note that the oscillations are in-phase, since these cost less energy and are therefore the first to become unstable; their frequency corresponds quantitatively with the prediction of the stability analysis.

3.2 Results on images

In this Section, we show the results of river network extraction from a piece of a four-band colour infrared Quickbird image (60cm resolution) using E_G. We add to E_G a likelihood term $E_{\text{l}}(I, R)$ consisting of multivariate Gaussian models of the image in the region interior and exterior, with parameters learned by example. For implementation, we use the implicit 'phase field' framework [6]. This simplifies and speeds up the algorithm. We select HOAC parameter values from the phase diagram and then compute the corresponding phase field parameters [6]. Figure 5 shows a segmentation result. The parameter values were $(w_0, d, \lambda_C, \alpha_C, \beta_C) = (5, 5.67, 80, 16.91, 8.77)$.

4 Conclusion

We have calculated the phase diagram of a bar under a higher-order active contour energy via a stability analysis, and we have confirmed the relevance of the analysis via experiments. Aside from its intrinsic interest, the calculation enables the determination of model parameter values for hydrographic network extraction from

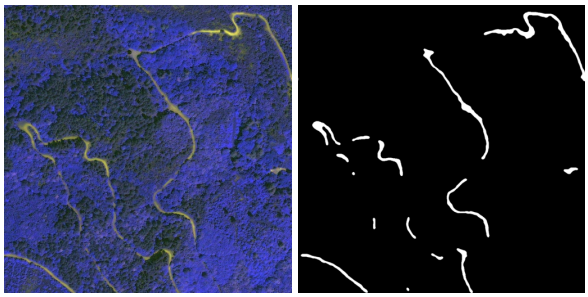

Figure 5. Image ©Spot Image; result.

VHR remote sensing images. This leads to the successful extraction of hydrographic networks, although further work remains to be done on closing gaps.

Acknowledgments

The authors thank the French Space Agency (CNES) for the satellite image, and CNES, PACA, the MUSCLE Network of Excellence (www.muscle-noe.org), and INRIA Associated Team SHAPES (www-sop.inria.fr/ariana/Projets/Shapes/index.html) for partial financial support.

References

[1] D. Cremers, M. Rousson, and R. Deriche. A review of statistical approaches to level set segmentation: Integrating color, texture, motion and shape. *Int. J. Comput. Vision*, 72(2):195–215, 2007.

[2] A. El Ghoul, I. H. Jermyn, and J. Zerubia. Diagramme de phase d'une énergie de type contours actifs d'ordre supérieur : le cas d'une barre longue. In *Reconnaissance des Formes et Intelligence Artificielle (RFIA)*, Amiens, France, Jan. 2008.

[3] P. Horvath, I. Jermyn, Z. Kato, and J. Zerubia. A higher-order active contour model for tree detection. In *Proc. International Conference on Pattern Recognition (ICPR)*, Hong Kong, Aug. 2006.

[4] M. Kass, A. Witkin, and D. Terzopoulos. Snakes: Active contour models. *International Journal of Computer Vision*, 1(4):321–331, 1988.

[5] M. Rochery, I. Jermyn, and J. Zerubia. Higher order active contours. *International Journal of Computer Vision*, 69(1):27–42, 2006.

[6] M. Rochery, I. H. Jermyn, and J. Zerubia. Phase field models and higher-order active contours. In *Proc. IEEE International Conference on Computer Vision (ICCV)*, Beijing, China, Oct. 2005.

[7] A. Srivastava, S. Joshi, W. Mio, and X. Liu. Statistical shape analysis: Clustering, learning, and testing. *IEEE Transactions on Pattern Analysis and Machine Intelligence*, 27(4):590–602, 2003.